Effects of nuclear motion on the ionization-induced terahertz radiation of H_2^+ in intense few-cycle laser pulses

Shan Xue, Hongchuan Du,* Yue Xia, and Bitao Hu†
School of Nuclear Science and Technology, Lanzhou University, Lanzhou 730000, China
(Received 23 April 2015; published 22 July 2015)

We examine the residual current to investigate the conversion efficiency from the few-cycle laser pulse into the terahertz radiation of H_2^+ by solving the time-dependent Schrödinger equation in the non-Born-Oppenheimer approach. It is found that the nuclear motion and high vibrational states will improve the optical-to-terahertz conversion efficiency significantly, while with the increasing of the laser intensity, ionization saturation will suppress the effects of moving nuclei. Moreover, based on the dependence of the residual current on the delay time of the nuclear vibration, we conclude that the terahertz signal may serve as a tool to probe the nuclear dynamics.

DOI: 10.1103/PhysRevA.92.013420 PACS number(s): 33.80.Wz, 42.50.Hz, 52.59.Ye

I. INTRODUCTION

In the study of the intense laser-induced phenomena, much attention has traditionally been paid to the generation of high-order harmonics (HHG) in order to obtain the attosecond pulses [1–5]. However, In recent years a new phenomenon, the ionization-induced conversion of femtosecond laser pulse into low-frequency radiation, particularly into the terahertz (THz) range, has become a research hot spot [6–9] and has been jointly researched with the HHG processes [10,11]. The physical mechanism can be explained as follows: When a laser field interacts with an atom or molecule, it first ionizes the electron, then the freed electron will acquire an oscillatory velocity along with a drift one. The latter is determined by the phase of the electric field at the moment of ionization. Due to the oscillatory velocity, the electron could recombine with its parent ion and emit high-frequency photon, namely the HHG, while the detached electron with the drift velocity will contribute to the macroscopic directional current. As a result, a residual-current density (RCD) will be retained in the produced plasma at the end of the laser pulse [12,13]. This directional RCD is an initial impetus to plasma polarization and excitation of the eigenoscillation. The oscillation stores energy which is proportional to the square root of the RCD, and then radiates THz waves under the condition of a rather dense laser-produced plasma into the environment [7,8].

This ionization-induced THz radiation was initially proposed as a comparatively simple way to monitor the carrier-envelope phase (CEP) of few-cycle laser pulses, for the RCD is quite sensitive to the variation of the CEP [6,8]. In fact, it also provides a way for the generation of high-power THz waves. From the mechanism mentioned above, one can see that the key to a higher conversion efficiency is to break the symmetry of the ionization process, which has been done in several works: (i) by using few-cycle laser pulses [7,8,14]; (ii) by ionization with two-color or multicolor laser fields [15–19], and (iii) by using asymmetric potential provided by oriented heteronuclear molecules [20].

For laser-molecule interaction, the situations are more complex than that in atoms because of additional degrees of freedom, for example, nuclear motion, different orientations with respect to the laser field, and so on. All of these have been extensively studied in the HHG process [21–26]. However, to our best knowledge, the influence of nuclear motion has been hardly reported in the ionization-induced radiation of THz frequency range so far. So in this work, we study how the nuclear motion and the initial conditions (different vibrational states, initial nuclear position, and velocity) affect the optical-to-THz conversion efficiency of the simplest diatomic molecule H_2^+ and its isotopomers by solving the one-dimensional (1D) time-dependent Schrödinger equation (1 D-TDSE) in the non-Born-Oppenheimer approach (NBOA) [13]. We conclude that the THz signal may be used as a tool to probe the nuclear dynamics. Moreover the quantum-mechanical numerical calculation allows us to explore all stages of electron-nuclear dynamics, such as atom ionization, Coulomb field of the nucleus, spread of the wave packet, electron-ion scattering, and so on.

II. THEORETICAL METHODS

Since the alignment of molecules is nowadays possible experimentally [27,28], we assume the laser field is linearly polarized along the molecular orientation. To avoid the extensive calculation of full dimension, the 1D-TDSE is adopted, which is solved numerically by using the split-operator method [29]. After neglecting the center-of-mass motion [30], it can be written as (atomic units are used throughout)

$$i\frac{\partial}{\partial t}\psi(z,R,t) = [H_n(R) + H_{el}(z,R,t)]\psi(z,R,t), \qquad (1)$$

where

$$H_n(R) = -\frac{1}{m_p}\frac{\partial}{\partial R^2} + \frac{1}{R}, \qquad (2)$$

$$H_{el}(z,R,t) = -\frac{2m_p + m_e}{4m_p m_e}\frac{\partial^2}{\partial z^2} + V_c(z,R) + V_l(z,t). \qquad (3)$$

The soft-Coulomb potential of H_2^+ is $V_c(z,R) = -\frac{1}{\sqrt{(z-R/2)^2+1}} - \frac{1}{\sqrt{(z+R/2)^2+1}}$, and the laser-molecule

*duhch@lzu.edu.cn
†hubt@lzu.edu.cn

interaction is given by $V_l(z,t) = -\frac{2m_p+2m_e}{2m_p+m_e} zE(t)$. Here R is the internuclear distance. m_e and m_p are the electron and proton masses ($m_e = 1$, $m_p = 1836$), respectively. z is the electronic coordinate with respect to the center of mass of the two nuclei. $E(t)$ is the linearly polarized laser field and it reads

$$E(t) = E_0 \cos(\pi t/\tau)^2 \sin(\omega t + \phi), \tag{4}$$

where E_0 is the amplitude, ω is the carrier frequency, τ is the total pulse duration, and ϕ is the CEP of the driving pulse. In the calculation, ω and τ are chosen to be 0.057 a.u. (wavelength 800 nm) and $3T_0$ (T_0 is the optical period of 800 nm), respectively. And the peak intensity of the laser pulse is set to be higher than 10^{15} W/cm^2, because the residual current is quite small in the symmetric potential at lower intensity.

The residual current observed at the end of the pulse can be found via the equation

$$j(t) = eN_g \int_{-\infty}^{t} a(t')dt', \tag{5}$$

where N_g is the initial density of the molecules and $a(t)$ is the dipole acceleration, which can be obtained on the use of the Ehrenfest theorem [31]. For a low degree of ionization, a fast oscillating current density of the electrons staying in the bound states can be significant. In order to filter it out, we continue our calculation for another 50 optical cycles after the end of the pulse, then the calculated residual current is averaged over these 50 cycles. As was done in Ref. [12], the residual current was normalized to the maximum value of the oscillatory current, $j_{\rm osc} = eN_g V_{\rm osc} = e^2 N_g E_0/(m\omega^2)$, excited in the emerging plasma by the laser field. Then the normalized residual current $j_{\rm norm} = j_{\rm res}/j_{\rm osc}$ will not depend on the gas density and can characterize the optical-to-THz conversion efficiency in the plasma formation stage.

III. RESULTS AND DISCUSSIONS

A. Effects of nuclear motion

Figure 1 shows the CEP dependencies of the nomalized RCD of H_2^+, D_2^+, and X_2^+ (X is a virtual isotope, which is five times heavier than that of H) with the pulse intensity $I = 1 \times 10^{15}$ W/cm^2. For comparison, the result calculated with the Born-Oppenheimer approximation (BOA) for H_2^+ is also given, whose internuclear distance is "frozen" and set to be the average internuclear separation of the lowest vibrational state of X_2^+. It can be seen that the shapes of the dependencies $j_{\rm norm}(\phi)$ for NBOA and BOA are similar and the optimal CEPs $\phi_{\rm opt}$ are also the same ($\phi_{\rm opt} = 0.8\pi$), at which residual currents reach their maximums. However, the only differences are the values of them at each CEP. Moreover, as the absolute value of the normalized RCD increases with the change of CEP, the differences between NBOA and BOA are basically getting larger for all three isotopomers. Especially at the optimal CEPs, the differences get the largest. For example, the relative difference [|($j_{\rm norm}$(NBOA)-$j_{\rm norm}$(BOA)/$j_{\rm norm}$(BOA)|] of H_2^+ at $\phi_{\rm opt} = 0.8\pi$ is 21.89%, which means that the conversion efficiency could be improved by about 10% in the stage of plasma generation. However, as the isotopomer becomes heavier, the differences between BOA and NBOA decreases gradually. To be noted, this amplification effect of the conversion efficiency is not limited by the selection of pulse parameters and can be found in other cases of laser pulse. Thus we can say that the optical-to-THz conversion efficiency could be improved greatly near the optimal CEP for light isotope by considering nuclear motion.

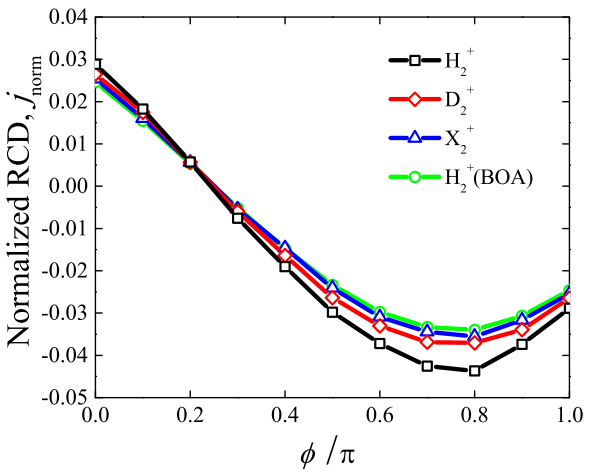

FIG. 1. (Color online) Normalized RCD $j_{\rm norm}$ as a function of the CEP ϕ for H_2^+, D_2^+, X_2^+, and H_2^+ (BOA) at $I = 1 \times 10^{15}$ W/cm^2.

To justify this amplification effect, we study the instantaneous ionization rate (IIR) introduced in [32], which is defined as $\Gamma(t) = \frac{-2E_{\rm Im}(t)}{N(t)}$. Here $E_{\rm Im}$ is the imaginary part of the instantaneous electronic energy and $N(t)$ is the instantaneous norm in the absorbing region which is set at $-30 \leqslant z \leqslant 30$ in our calculation. So it will take time for the electronic wave packet (EWP) to reach the borders during the interaction. EWP is the spatial distribution of the electron probability density which is the modulus squared of the wave function at each z point. Figure 2(a), which can be a good illustration, depicts the evolution of the EWP at $I = 1 \times 10^{15}$ W/cm^2, $\phi_{\rm opt} = 0.8\pi$ in the BOA case. The dotted pink lines indicate the absorbing borders. Figure 2(c) shows the corresponding IIRs in both the BOA and NBOA cases. As can be seen, there are two peaks located at around $0.03T_0$ and $0.5T_0$ which mainly contribute to the residual current. This is consistent with the redder (dark gray) parts near the borders shown in Fig. 2(a). It is worth noting that the positive (negative) value of the IIR corresponds to the incoming (outgoing) of the electron to (from) the region. And the oscillation of the second peak is due to the incoming part of the EWP at the $+z$ direction. Moreover, the ionization rate of the lighter isotopomer is higher than that of the heavier isotopomer and the "frozen" nuclei case, which can enlarge the asymmetry of the ionization process. Especially for H_2^+, the second peak shows the highest ionization rate, indicating that more electrons will be ejected at this time to contribute to the macroscopic current, leading to a stronger plasma polarization for the THz radiation. Therefore, the amplification effect observed in Fig. 1 can be justified by the significant differences of IIRs. Figure 2(b) shows the time-dependent average internuclear separations $\langle R \rangle$ in the NBOA case. At first, they are all located near the equilibrium position $2.6a_0$ (a_0 is the Bohr radius). Then in the process of interaction with the laser field, $\langle R \rangle$ increases much faster for the lighter isotopomer H_2^+ than for the other two isotopomers. For example, the internuclear distance of

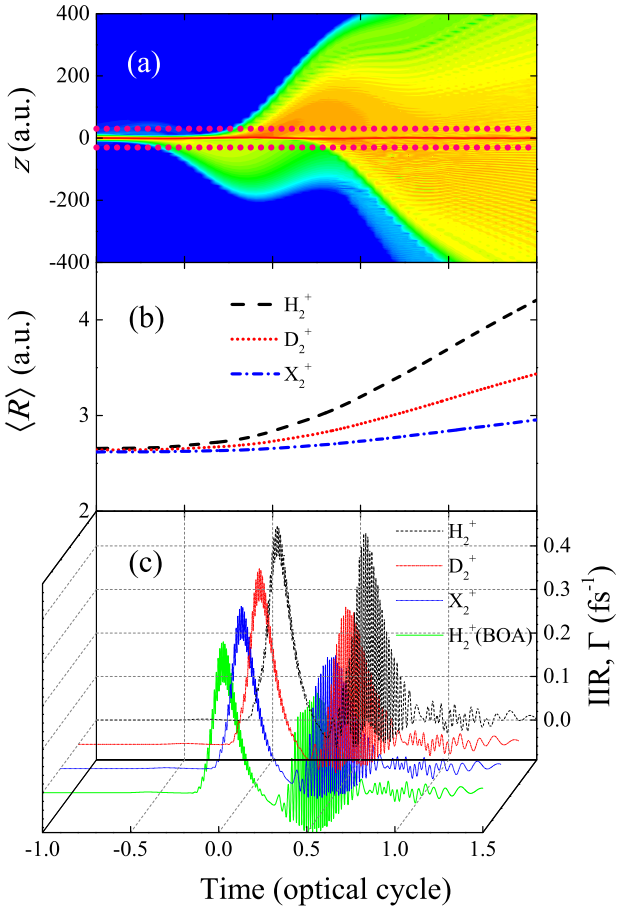

FIG. 2. (Color online) (a) The propagation of EWP of H_2^+ (BOA) evolving over time at $I = 1 \times 10^{15}$ W/cm^2, $\phi_{opt} = 0.8\pi$. Dotted pink lines indicate the absorbing borders used in the IIR calculation. (b) The average internuclear separations $\langle R \rangle$ of H_2^+, D_2^+, and X_2^+ in the NBOA case at the same parameters. (c) The corresponding IIRs as function of time for H_2^+ (dashed black line), D_2^+ (dotted red line), X_2^+ (dash dotted blue line), and H_2^+ (BOA) (solid green line).

X_2^+ is almost unchanged. This is because heavier nuclei get smaller acceleration and move slowly in the electric field. The increasing of the internuclear separation will lower the ionization potential of the molecule that makes the electron tunnel easier [25], which is consistent with the ionization rates shown in Fig. 2(c). Since the electronic structures of different isotopomers used in this work are similar, we justify that nuclear motion is responsible for the difference of the ionization rate and further influences the optical-to-THz conversion efficiency. In addition, the increasing of $\langle R \rangle$ should be attributed mainly to the bond softening and the Coulomb explosion after the single electron ionized [33].

In the following, we further study the nuclear motion effects at higher laser intensities. Figure 3 shows the dependencies of the maximum absolute value of the normalized RCD $j_{max} = |j_{norm}(\phi_{opt})|$ of H_2^+ on the laser intensity in NBOA and BOA. The relative differences are also presented near the data points. By zooming in on the point $I = 1 \times 10^{15}$ W/cm^2, it can be seen that the amplification effect is remarkable at lower intensities. However, as the laser intensity grows, the relative

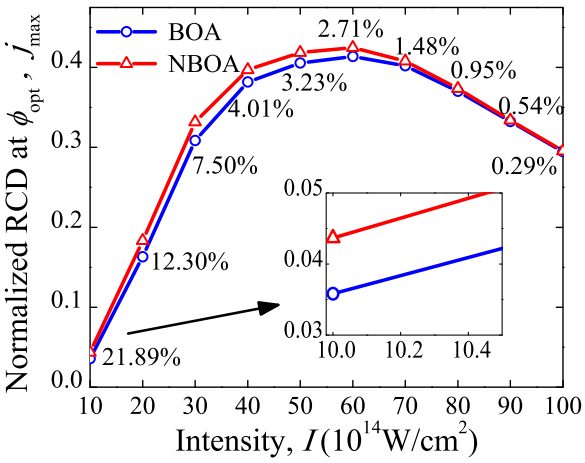

FIG. 3. (Color online) The maximum absolute value of normalized RCD j_{max} as function of the laser intensity I for NBOA and BOA cases. The relative differences are given near the data points.

differences are getting smaller and smaller, which means an attenuation of the amplification effect. Meanwhile, the residual current first increases rapidly, then declines slowly, which is consistent with the previous works [12]. As stated above, the ionization process can be sensitively influenced by the nuclear motion. For large intensity region, ionization mostly occurs at the rising part of the pulse and tends to be saturated before the nuclei separation stretches to some distance. For this reason, the nuclear motion will not influence the ionization process at some higher intensities, not to mention improving the conversion efficiency. For even higher intensities, the ionization mechanism will be in the over-the-barrier ionization regime, then the nuclear motion will basically play no role in the ionization process. In a word, the normalized RCD obtained from NBOA and BOA will tend to be equal eventually as the intensity increases.

Here we also present similar results as in Fig. 2 for an intensity of $I = 1 \times 10^{16}$ W/cm^2. Figure 4(a) shows the evolution of the EWP at the optimal CEP $\phi_{opt} = \pi$ in BOA. The dotted pink lines indicate the positions of the absorbing borders. Figure 4(b) shows the time-dependent average internuclear separations, which spread to larger distances compared with Fig. 2(b). Figure 4(c) depicts the corresponding IIRs of H_2^+, D_2^+, X_2^+, and H_2^+ (BOA). As can be found, first, the ionization rates are much higher than that at $I = 1 \times 10^{15}$ W/cm^2, leading to the increasing of the normalized RCD. Second, the ionization occurs earlier, which can also be seen intuitively from Fig. 4(a). Third, the four IIRs are basically identical, which can explain the tiny relative difference shown in Fig. 3. As stated above, the over-the-barrier ionization mechanism will dominate the process at such a high laser intensity, and the electrons are mostly ionized in the rising part of the pulse, so the nuclear motion will hardly affect the ionization process.

B. Effects of different initial conditions

Next, we investigate how the initial vibrational states influence the optical-to-THz conversion efficiency. The respective $j_{norm}(\phi)$ of H_2^+ for the initial states $v = 0$–5 are

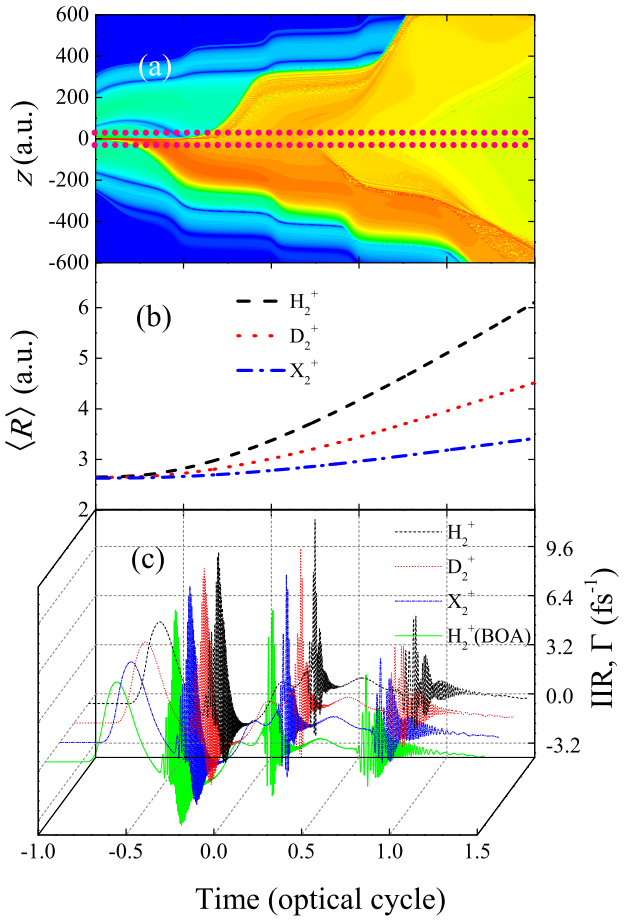

FIG. 4. (Color online) (a) The propagation of EWP of H_2^+ (BOA) evolving over time at $I = 1 \times 10^{16}$ W/cm^2, $\phi_{opt} = \pi$. Dotted pink lines indicate the absorbing borders. (b) The average internuclear separations $\langle R \rangle$ of H_2^+, D_2^+, and X_2^+ in the NBOA case. (c) The corresponding IIRs as function of time for H_2^+ (dashed black line), D_2^+ (dotted red line), X_2^+ (dash dotted blue line), and H_2^+ (BOA) (solid green line).

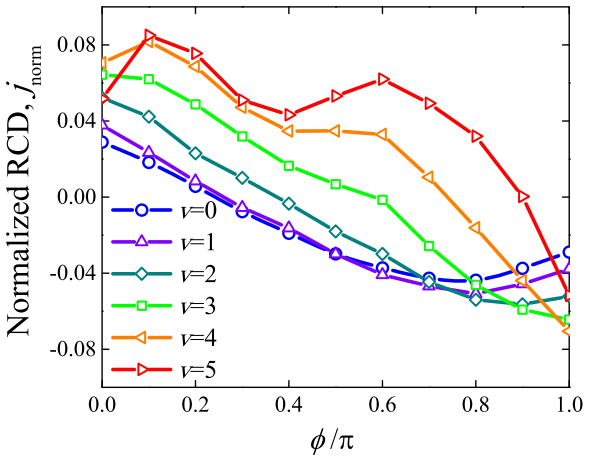

FIG. 5. (Color online) Normalized RCD of H_2^+ at different vibrational states as function of the CEP ϕ at $I = 1 \times 10^{15}$ W/cm^2.

presented in Fig. 5. The laser intensity is chosen to be $I = 1 \times 10^{15}$ W/cm^2. It can be seen that the shape of the dependence $j_{norm}(\phi)$ changes gradually as the v number rises, and finally gets two humps near $\phi = 0.1\pi$ and 0.6π. Meanwhile the THz conversion efficiency is also improved. Here we depict the evolution of the EWPs and the IIRs for $v = 0$ and 5 in Fig. 6 to research the underlying physical reason. It can be seen from Figs. 6(c) and 6(d) that the IIR of $v = 5$ is one order higher than that of $v = 0$, but the most important is that the ionization occurs earlier for $v = 5$ at each peak. As is shown apparently in the dashed blue box in Fig. 6(b), these earlier ionized electrons show higher time gradient, namely rapid drift velocity, which could influence the residual current greatly after the contribution of each half optical cycle at the end of the laser pulse. This phenomenon can be explained as follows: for higher v, the initial internuclear separation is larger and the ionization potential is lower. At this point, a relatively small instantaneous intensity could ionize the electron, therefore the ionization time shifted forward. While for lower vibrational states with higher ionization potentials, it will need a stronger instantaneous intensity near the peak of each half cycle for the electron to be ionized or take a long time for the internuclear separation to stretch to a critical distance to trigger the enhanced ionization (EI) [33–35]. In addition, each peak of the ionization rate for $v = 5$ has a double-peak or multipeak structure. This is because the laser field induces a coupling of different electronic states. Then the populations of different states will oscillate during the interaction process, which results in the peak splitting of the ionization rate. To be noted is that this phenomenon is distinct from the intracycle interference, which is caused by the superimposing of the EWPs ejected around two adjacent optical peaks [36] and leads to the fine splitting at each peak. In a word, all of this suggests that the optical-to-THz conversion efficiency will be improved significantly by employing higher vibrational states.

In experiment, vibrational states can be excited by using impulsive-stimulated Raman scattering (ISRS) [37,38]. Then the molecule will freely oscillate due to the superposition

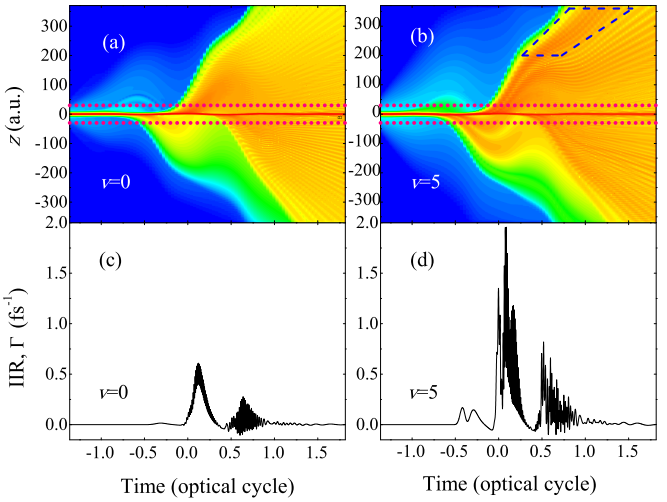

FIG. 6. (Color online) The EWPs (a), (b) evolving over time for $v = 0$, 5 and the corresponding IIRs (c), (d) at $I = 1 \times 10^{15}$ W/cm^2, $\phi = 0.6\pi$. Dotted pink lines are the absorbing borders. The EWP shown in the dashed blue box indicates the earlier ionized electrons.

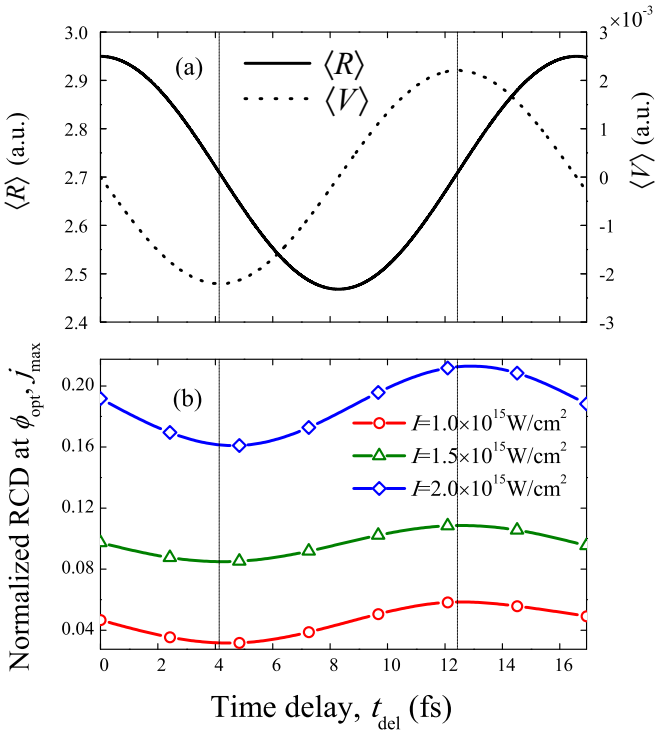

FIG. 7. (Color online) (a) The average internuclear separation $\langle R\rangle$ and the average nuclear velocity $\langle V\rangle$ as function of the time without interacting with the laser field. (b) The dependencies of the absolute normalized RCD on the time delay $t_{\rm del}$ at $I = 1,1.5,2 \times 10^{15}$ W/cm^2 at their optimal CEPs. The vertical dashed lines are located at $t_{\rm del} = 4.14$ and 12.43 fs, which indicate the times when nuclei reach their forward and reverse maximum velocities, respectively.

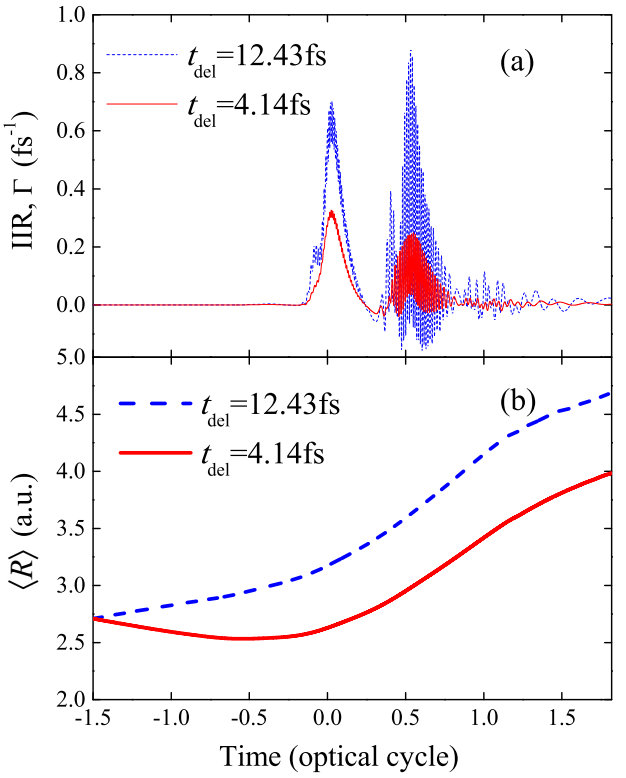

FIG. 8. (Color online) The IIRs (a) and the average internuclear separations $\langle R\rangle$ (b) as a function of time with two cases of time delay 4.14 fs (solid red line) and 12.43 fs (dashed blue line) at $I = 1 \times 10^{15}$ W/cm^2.

of different vibrational states. Here we show results calculated with the nuclear initial wave function prepared as a superposition of the two lowest vibrational states ($v = 0$, 1) with the same probabilities to study the effects of nuclear vibration on the THz conversion efficiency. Figure 7(a) shows the average internuclear separation and the average nuclear velocity changing without interacting with the laser pulse for about one period of the vibration (∼16.6 fs). By turning on the laser pulse at different delay time $t_{\rm del}$, we calculated the absolute value of the normalized RCD at three different laser intensities $I = 1,1.5,2 \times 10^{15}$ W/cm^2 at their optimal CEPs, respectively. As can be seen in Fig. 7(b), the residual currents are modulated by the nuclear vibration and, for different laser intensities with $\phi_{\rm opt}$, they have a similar trend with $t_{\rm del}$ increasing. Moreover, the absolute values reach maximums near the time when $\langle R\rangle$ takes the equilibrium value and the nuclei move away from each other at the maximum velocity. However, at the same nuclear position but in the opposite direction of nuclear velocity, the values reach their minimums. As we did earlier, the average internuclear separations and the IIRs as a function of time with two delay times $t_{\rm del} = 4.14$ and 12.43 fs are presented in Fig. 8, corresponding to the maximum and minimum nuclear velocities. It can be seen that the IIR of $t_{\rm del} = 12.43$ fs is more than twice as high as $t_{\rm del} = 4.14$ fs for both peaks, especially the second one. Furthermore, the double-peak structures show again, whose physical mechanism has been pointed out above. Figure 8(b) shows that the internuclear separations are both $2.7a_0$ at first, then one decreases for the $t_{\rm del} = 4.14$-fs case due to the negative initial velocity. While for the $t_{\rm del} = 12.43$-fs case, the separation keeps increasing due to the positive initial velocity. At the end, they differ by about $0.7a_0$. Since larger internuclear separation makes ionization easier, this significant difference definitely leads to the change of the ionization rate. Therefore we conclude that, during the ionization process, initial positive velocity always leads to a larger internuclear separation than an initial negative velocity, thus to improve the ionization rate. So the initial nuclear velocity plays a more important role than the initial nuclear position in the optical-to-THz wave conversion process. Therefore, based on the nuclear velocity dependence of the THz signal, we conclude that the nuclear dynamics may be probed.

IV. CONCLUSION

In conclusion, we have investigated the effects of nuclear motion on the optical-to-THz wave conversion efficiency by solving the 1D-TDSE with and without the Born-Oppenheimer approximation. Our results show that when nuclear motion is taken into account, higher conversion efficiency could be obtained for a light isotope. As the laser intensity increases, the amplification effect will become attenuated due to the ionization saturation in the rising edge of the pulse. Then we investigate how the initial conditions affect the conversion

efficiency. It is found that the CEP dependent residual current will change apparently for higher vibrational states, which should be paid attention to for monitoring the CEP of few-cycle laser pulses. Considering the nuclear vibration, the initial nuclear position and velocity can also modulate the residual current significantly, which can serve as a tool to probe the nuclear dynamics. In turn, by producing the initial wave packets with higher vibrational states and separated nuclear velocity, the optical-to-THz conversion efficiency will be improved as well. In addition, the 1D-TDSE has been widely used in previous works when considering nuclear motion [22,23,39–42], which could overestimate the recollision and rescattering effects relative to full-dimensional calculation. While for the generation of the macroscopic residual current, electron rescattering effects play a minor role according to the former full-dimension simulation [19]. Thus we believe that the results obtained in the reduced dimension are reliable and will be realized in the future experiment.

ACKNOWLEDGMENTS

This work was supported by the National Natural Science Foundation of China (Grants No. 11404153, No. 11135002, No. 11175076, No. 11475076, and No. 11405077) and the Fundamental Research Funds for the Central Universities of China (Grants No. lzujbky-2014-10, No. lzujbky-2014-13, and No. lzujbky-2014-14).

[1] P. B. Corkum and F. Krausz, Nat. Phys. **3**, 381 (2007).
[2] Z. N. Zeng, Y. Cheng, X. H. Song, R. X. Li, and Z. Z. Xu, Phys. Rev. Lett. **98**, 203901 (2007).
[3] Y. Pan, S. F. Zhao, and X. X. Zhou, Phys. Rev. A **87**, 035805 (2013).
[4] H. C. Du, Y. Z. Wen, X. S. Wang, and B. T. Hu, Opt. Express **21**, 21337 (2013).
[5] H. C. Du and B. T. Hu, Phys. Rev. A **84**, 023817 (2011).
[6] M. Kreß, T. Löffler, M. D. Thomson, R. Dörner, H. Gimpel, K. Zrost, T. Ergler, R. Moshammer, U. Morgner, J. Ullrich, and H. G. Roskos, Nat. Phys. **2**, 327 (2006).
[7] V. B. Gildenburg and N. V. Vvedenskii, Phys. Rev. Lett. **98**, 245002 (2007).
[8] H. C. Wu, J. Meyer-ter-Vehn, and Z. M. Sheng, New J. Phys. **10**, 043001 (2008).
[9] T. I. Oh, Y. S. You, N. Jhajj, E. W. Rosenthal, H. M. Milchberg, and K. Y. Kim, New J. Phys. **15**, 075002 (2013).
[10] D. Zhang, Z. Lü, C. Meng, X. Du, Z. Zhou, Z. Zhao, and J. Yuan, Phys. Rev. Lett. **109**, 243002 (2012).
[11] Z. Lü, D. Zhang, C. Meng, X. Du, Z. Zhou, Y. Huang, Z. Zhao, and J. Yuan, J. Phys. B: At. Mol. Opt. Phys. **46**, 155602 (2013).
[12] A. A. Silaev and N. V. Vvedenskii, Phys. Rev. Lett. **102**, 115005 (2009).
[13] A. A. Silaev, M. Yu. Ryabikin, and N. V. Vvedenskii, Phys. Rev. A **82**, 033416 (2010).
[14] K. Y. Kim, J. H. Glownia, A. J. Taylor, and G. Rodriguez, Opt. Express **15**, 4577 (2007).
[15] K. Y. Kim, A. J. Taylor, J. H. Glownia, and G. Rodriguez, Nat. Photon. **2**, 605 (2008).
[16] N. Karpowicz and X. C. Zhang, Phys. Rev. Lett. **102**, 093001 (2009).
[17] J. Dai, N. Karpowicz, and X. C. Zhang, Phys. Rev. Lett. **103**, 023001 (2009).
[18] I. Babushkin, S. Skupin, A. Husakou, C. Köhler, E. Cabrera-Granado, L. Bergé, and J. Herrmann, New J. Phys. **13**, 123029 (2011).
[19] L. N. Alexandrov, M. Yu. Emelin, and M. Yu. Ryabikin, Phys. Rev. A **87**, 013414 (2013).
[20] A. Zavriyev, P. H. Bucksbaum, J. Squier, and F. Saline, Phys. Rev. Lett. **70**, 1077 (1993).
[21] M. Lein, Phys. Rev. Lett. **94**, 053004 (2005).
[22] Y. H. Guo, H. X. He, J. Y. Liu, and G. Z. He, J. Mol. Struct.: THEOCHEM **947**, 119 (2010).
[23] J. Zhao and Z. X. Zhao, Phys. Rev. A **78**, 053414 (2008).
[24] H. C. Du, L. Y. Luo, X. S. Wang, and B. T. Hu, Phys. Rev. A **86**, 013846 (2012).
[25] M. Lein, N. Hay, R. Velotta, J. P. Marangos, and P. L. Knight, Phys. Rev. Lett. **88**, 183903 (2002).
[26] J. Itatani, J. Levesque, D. Zeidler, H. Niikura, H. Pépin, J. C. Kieffer, P. B. Corkum, and D. M. Villeneuve, Nature (London) **432**, 867 (2004).
[27] C. Vozzi, M. Negro, F. Calegari, G. Sansone, M. Nisoli, S. D. Silvestri, and S. Stagira, Nat. Phys. **7**, 822 (2011).
[28] C. Vozzi, F. Calegari, E. Benedetti, J.-P. Caumes, G. Sansone, S. Stagira, M. Nisoli, R. Torres, E. Heesel, N. Kajumba, J. P. Marangos, C. Altucci, and R. Velotta, Phys. Rev. Lett. **95**, 153902 (2005).
[29] M. D. Feit, J. A. Fleck Jr, and A. Steiger, J. Comput. Phys. **47**, 412 (1982).
[30] J. R. Hiskes, Phys. Rev. **122**, 1207 (1961).
[31] K. Burnett, V. C. Reed, J. Cooper, and P. L. Knight, Phys. Rev. A **45**, 3347 (1992).
[32] M. Vafaee, H. Sabzyan, Z. Vafaee, and A. Katanforoush, Phys. Rev. A **74**, 043416 (2006).
[33] S. Chelkowski, A. Conjusteau, T. Zuo, and A. D. Bandrauk, Phys. Rev. A **54**, 3235 (1996).
[34] T. Zuo, S. Chelkowski, and A. D. Bandrauk, Phys. Rev. A **48**, 3837 (1993).
[35] T. Zuo and A. D. Bandrauk, Phys. Rev. A **52**, R2511(R) (1995).
[36] D. G. Arbó, K. L. Ishikawa, K. Schiessl, E. Persson, and J. Burgdörfer, Phys. Rev. A **81**, 021403(R) (2010).
[37] A. M. Weiner, D. E. Leaird, G. P. Wiederrecht, and K. A. Nelson, Science **247**, 1317 (1990).
[38] M. Wittmann, A. Nazarkin, and G. Korn, Phys. Rev. Lett. **84**, 5508 (2000).
[39] W. Qu, Z. Chen, Z. Xu, and C. H. Keitel, Phys. Rev. A **65**, 013402 (2001).
[40] A. D. Bandrauk, S. Chelkowski, and H. Lu, J. Phys. B: At. Mol. Opt. Phys. **42**, 075602 (2009).
[41] X. Y. Miao and J. Han, Spec. Lett. **47**, 471 (2014).
[42] X. L. Ge, T. Wang, J. Guo, and X. S. Liu, Phys. Rev. A **89**, 023424 (2014).